Geomorphology 454 (2024) 109163

Contents lists available at ScienceDirect

Geomorphology

journal homepage: www.journals.elsevier.com/geomorphology

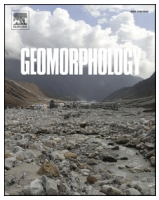

Multivariate analysis of inlet morphodynamics: The mixed sand-gravel ebb-tidal delta of Deben Estuary, Suffolk

Jie Gong *, Helene Burningham

Department of Geography, University College London, London, UK

ARTICLE INFO

Keywords:
Multivariate analysis
Inlet morphodynamics
Bathymetric analysis
Volumetric analysis
Wave climate
Metocean forcing

ABSTRACT

The morphodynamics of inlets and ebb-tidal deltas often exhibit cyclic behaviour, controlled by wave-tide interactions and the influence of these on sediment-bypassing processes. Variation in the form and timing of inlet dynamics can occur in response to changes in the key sediment transport processes and sediment supply, and particularly the relative dominance of differential wave direction driving alongshore sediment transport. This paper investigates the morphodynamics of the Deben ebb-tidal delta through multivariate analysis of multi-annual bathymetry and metocean parameters covering the period 1991 to 2023. Results show that sediment bypassing and associated morphological change in this ebb-tidal delta follows variable behaviour mid-cycle, leading to change in the morphology and configuration of the ebb-delta from cycle to cycle. In the most recent cycle (since 2003), delta volume followed a stepwise growth driven by sediment influx periods, evident primarily in the updrift shoal, followed by cross-shore redistribution. Interannual variability in wave climate was clustered into four groups that capture the relative balance between the dominant NE and SW forcing. Sediment influx periods are mostly associated with subdued SW and increased NE forcing, but the summer and winter NE wave climate play different roles on the up- and downdrift, and upper and lower components of the ebb-delta system. Tide level has increased in the last 33 years, which is strongly correlated with ebb-delta volume increase. Wave and tide conditions have discrete and independent effects on the ebb-tidal delta, whereas wave-tide interactions do not significantly change these underlying influences.

1. Introduction

Typically, tidal inlets interrupt barrier island chains, providing tidal connection and conduits of water and sediment exchange between marine and estuarine environments (McBride et al., 2022). Tidal inlets are also found on more complex shorelines where sediment has accumulated at the mouth of estuarine valley, and where tidal currents are responsible for maintaining the connection between estuary and open sea. Inlets play a significant role in moderating local longshore sediment transport, acting as a sediment sink as well as a source (De Swart and Zimmerman, 2009; FitzGerald et al., 2002; Hicks and Hume, 1996; McBride et al., 2022; Oertel, 1988). The sedimentary systems of inlets have been well described (Hayes, 1980; Hayes and FitzGerald, 2013), and those occurring on mesotidal coasts comprise an ebb-tidal delta seawards and possibly a flood-tidal delta landwards of the tidal inlet throat. The morphodynamics of tidal inlets is the mutual association mediated by feedback mechanisms between hydrodynamics, sediment transport, grain size, and morphological change (FitzGerald, 1988), which also explains their morphological diversity.

Ebb-tidal deltas frequently exhibit progressive and/or cyclic channel-shoal behaviour, whereby ebb channels are deflected in the direction of sediment transport, which also drives the growth, form, migration, and shoreline-welding of (mostly intertidal) shoals (Burningham and French, 2006; FitzGerald, 1988; Ford and Dickson, 2018; Gaudiano and Kana, 2001; He et al., 2022; O'Connor et al., 2011; Ridderinkhof et al., 2016b). Both tidal currents and wave transformation are considered the main forces driving these processes. Tidal currents generally influence the broader organisation of sediment within the inlet system and the route of channels (Elias et al., 2006; FitzGerald, 1984; Herrling and Winter, 2018), whilst wave conditions determine the alongshore transport direction and supply of sediment, and the cross-shore development and movement of morphological features such as bars and berms. The local imbalance between the wave conditions and the nearshore bathymetry results in the evolution of shoals (Bertin et al., 2009; Dodet et al., 2013; Ridderinkhof et al., 2016a). The morphodynamics of the system determines the mechanisms by which sediment is

* Corresponding author.
E-mail address: jie.gong.19@ucl.ac.uk (J. Gong).

https://doi.org/10.1016/j.geomorph.2024.109163
Received 6 December 2023; Received in revised form 16 March 2024; Accepted 17 March 2024
Available online 20 March 2024

moved through the inlet system and the extent to which sediment is trapped within the delta, or bypassed to the adjacent shoreline (Beck et al., 2020).

Herrling and Winter (2018) reviewed previous studies and concluded three principal mechanisms of natural sandy inlet sediment bypassing. Bar welding refers to the ebb currents transporting sediment around the inlet throat to the ebb-tidal delta where alongshore currents drive the formation, migration, and welding of shoals to the downdrift coast (Bruun and Gerritsen, 1959; Elias et al., 2019; FitzGerald, 1982; Ridderinkhof et al., 2016a). Sediment recirculation takes place, where some of the mobile sediment volume is transported back into the inlet throat from the downdrift shoal, which can weaken the evidence of sediment bypassing (Elias et al., 2006; Elias and Hansen, 2013; FitzGerald, 1984; Hench and Luettich Jr., 2003; Herrling and Winter, 2014; Smith and FitzGerald, 1994). Ebb-delta periphery bypassing is when wave-driven sediments are moved along the margin of the ebb-tidal delta through migrating transverse bars from the updrift to the downdrift coast (Gaye and Walther, 1935), which occurs less at small tidal inlets without multiple ebb channels (Luck and Witte, 1974). Much of our understanding of inlet dynamics and sediment bypassing is informed directly by the multitude of studies on sandy systems, but these interactions and processes are more complex for inlets comprising a distinct gravel sediment population due to the role of grain size on sediment transport processes and morphology. Compared with waves and rivers, the capacity and competency of tidal currents in transporting gravel is reduced, meaning that the interaction between waves and tides in transporting sediment within mixed sediment inlets is considerably more complicated (Carter and Orford, 1993).

In studying these coastal morphodynamics, bathymetric data that captures the changing morphology is crucial in providing an intuitive view of morphological change. However, due to the shallow depth and morphological complexity of tidal inlet systems, bathymetric surveys covering whole inlet and ebb-delta area are challenging to undertake, and are thus often sparse over suitable spatial and temporal scales (Burvingt et al., 2022). Many good initial frameworks and conceptual models of the inlet and ebb-tidal delta morphodynamics have been proposed drawing from discrete bathymetric data, but limitations in temporal and spatial resolution make it difficult to verify conceptual models and statistically interrogate specific behaviour (Elias et al., 2019; Son et al., 2011). In recent years, satellite-derived bathymetry has been growing as a new direction of coastal analysis to solve the problem of limited bathymetric data (Almar et al., 2021; Burvingt et al., 2022; Geyman and Maloof, 2019). However, achieving a long-term bathymetric time series relies on older satellite sensors with lower spatial resolution, which might work for the analysis of shoreline change and large inlet systems (Ford and Dickson, 2018), but not in small to medium tidal inlets. Equally, unpiloted aerial and surface systems can provide high-resolution data, but the technology to deliver this at the scale of inlet systems is only recent, and these data do not cover longer time periods.

Limitations in data quality and/or availability makes the systematic and empirical analysis of ebb-tidal delta morphodynamics challenging. Bathymetric data have been acquired for the mixed sand-gravel Deben inlet (see Section 3.1) on the east coast of the UK, each spring for the last few decades, required to support the accurate re-positioning of navigation aids each year owing to the ongoing movement of channels and banks that form its ebb-tidal delta. These data capture morphological change across at least one completed ebb-tidal delta cyclic behaviour, which is estimated to take 10 to 30 years based on analyses of historical inlet geomorphology (Burningham and French, 2006). The conceptual understanding of ebb-tidal delta morphodynamics derived was drawn from disparate, multi-decadal bathymetric evidence over 180 years from hydrographic charts. Here, we utilise annual surveys from 1991 to 2023, and progress a multivariate approach to investigate the morphodynamics of a mixed sand-gravel tidal inlet. First, bathymetric digital elevation models (DEMs) are used to evaluate change in morphological behaviour of the ebb-tidal delta through two sediment-bypassing cycles. Second, volumetric analysis of the ebb-tidal delta is examined vertically and horizontally and underpins a multi-method statistical analysis of the co-evolution of morphology, wave climate, and tidal conditions.

2. Study site

The south-oriented tidal inlet at the mouth of the Deben estuary (Fig. 1) connects the spit-enclosed Deben estuary on the Suffolk coast (southeast England) to the southern North Sea. The Deben inlet system, also known as Woodbridge Haven, comprises a flood- and ebb-tidal delta landward and seaward respectively of a narrow (~ 180 m wide) inlet throat. The ebb-tidal delta, known locally as The Knolls, is formed of two main shoals each attached to the north and south inlet margins, which vary in size and shape as the main ebb-channel migrates within the ebb-delta. The adjacent shoreface seabed consists of broken shells, fine sand, and mud, where sub-marine river channels are filled with fine material; a London Clay shore platform outcrops in the low intertidal and subtidal zones to the north and south of the inlet (Wallingford, 2002). Sand and gravel are found throughout the inlet system and adjacent beaches, with an average ratio of 17 % sand to 83 % gravel, but the distribution is locally and spatially varied along- and cross-shore (Balaga, 2006; Burningham and French, 2006; Posford Duvivier, 1999).

The Deben inlet is classified as a tide-dominated meso-tidal inlet, whilst it is also subjected to complex longshore sediment transport processes and the storm wave climate of the southern North Sea (Burningham and French, 2006). The mean spring tidal range around the Deben entrance is 3.2 m (Hydrographic Hydrographic Office, 2000), and the estuary has a tidal length of around 18 km and tidal prism 12×10^6 m^3 (Burningham and French, 2006). Fluvial inputs to the Deben are very small relative to the size of the tidal exchange: mean flow of the river Deben at Naunton Hall (2 km upstream from the tidal limit at Ufford Mill) is about 0.78 m^3/s and at Mill River, which enters mid-estuary, is 0.15 m^3/s (NRFA, 2024). Sediment input from the catchment is negligible. The Deben inlet, between Bawdsey Quay and Felixstowe Ferry, is approximately 180 m wide, which limits wave propagation into the estuary. Whilst dredging is carried out to keep channels navigable in the upper reaches of the estuary, no maintenance of channel depths is required in the lower Deben estuary or inlet. Offshore, the average wave height is 0.97 m (1990–2023) and wave climate is bimodal where wave direction is predominately from the northeast (NE) or southwest (SW). The significant wave height (H_s) of SW waves is normally larger than NE waves ($H_{sSW} = 1.10$ m and $H_{sNE} = 0.88$ m) but with lower wave periods ($T_{pSW} = 4.19$ s and $T_{pNE} = 4.63$ s). Despite the bimodality and tendency for larger southerly waves, most of the coastal geomorphology of south Suffolk points to southward sediment transport dominance, and NE waves appear to drive longshore sediment transport from north to south (Burningham and French, 2017). Inshore tidal currents across the Suffolk shoreface are insufficient for the transport of sands and gravel (Leonardi and Plater, 2017).

Burningham and French (2006) proposed a conceptual model of inlet and ebb-tidal delta morphodynamics, comprising three phases within a cyclic behaviour. With the sediments imported by NE waves, the updrift shoal extends southward and the ebb-jet shifts from southeast-directed to south-directed. When the updrift shoal extends sufficiently that the tidal channel route becomes inefficient, the updrift shoal starts to breakdown. Ultimately, the updrift shoal is permanently breached and the ebb-channel shifts to a new position dividing the updrift shoal; and the abandoned channel is then consumed as the divided shoal welds to the adjacent downdrift shoreline. The time scale of one such cycle takes 10 to 30 years, whilst the unstable phase of breakdown to final breaching takes around two years (Burningham and French, 2006).

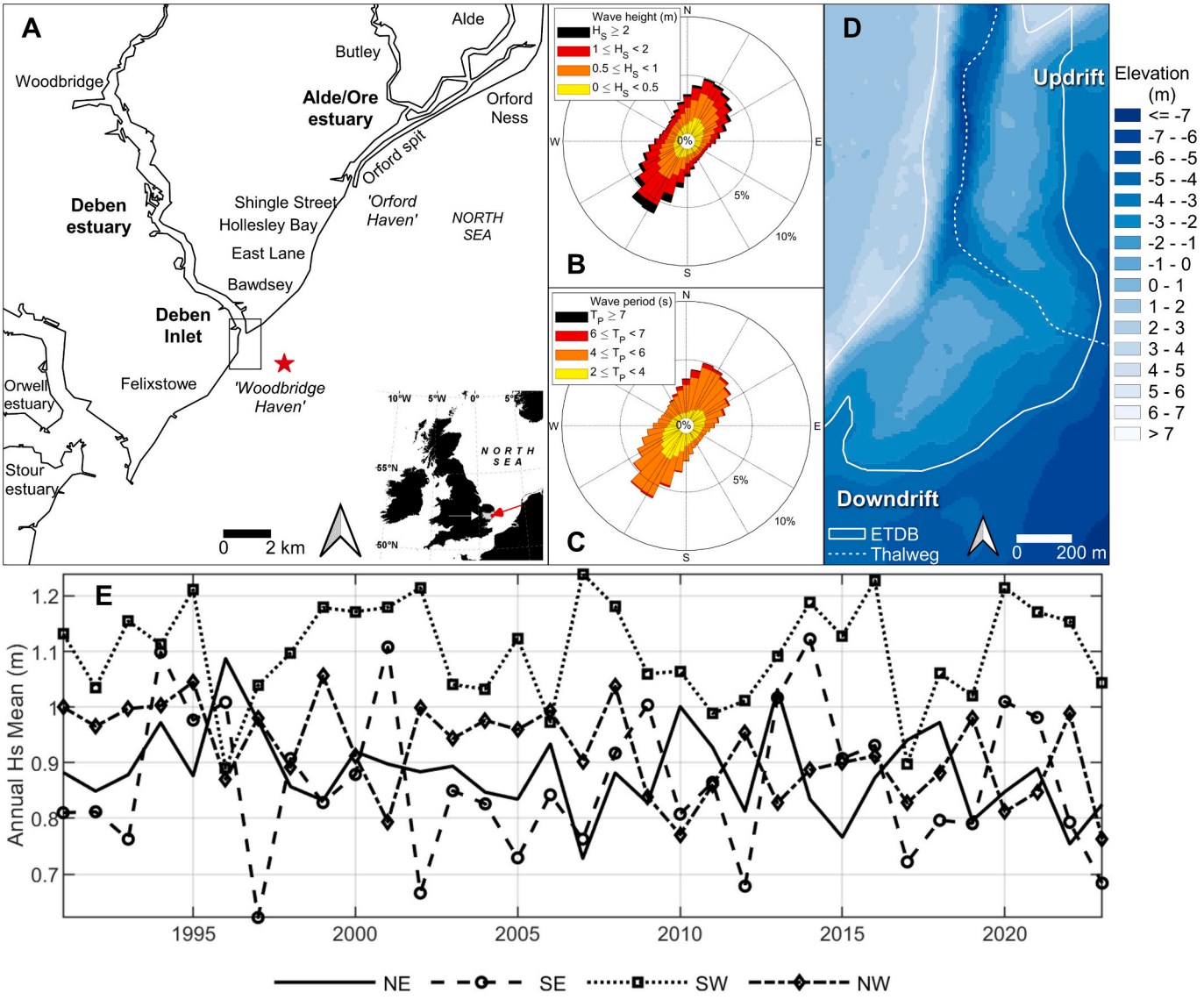

Fig. 1. Location of the Deben inlet (sometimes referred to as Woodbridge Haven (A) at the mouth of the Deben estuary in Suffolk, southeast England. Nearshore wave climate (significant wave height (B) and wave period (C)) over the period 1991–2023 from ERA5 (wave data point shown as star marker in A)) is strongly bidirectional. The inlet comprises a central low tide channel dividing up- and downdrift shorelines and ebb-delta shoals (ebb-tidal delta boundary (ETDB) and thalweg shown on the 2003 morphology in (D)) that move in a cycle from north to south despite a tendency for southerly waves to be larger than northerly waves (annual mean of the significant wave height (H_S) from NE, SE, SW and NW shown in (E)).

3. Methods

3.1. Bathymetry and volumetric analysis

Bathymetric surveys of estuary entrances around the UK are undertaken regularly by Trinity House to support their maritime navigation service. Serving as the General Lighthouse Authority for England, Wales, the Channel Islands, and Gibraltar, Trinity House is a charity dedicated to safeguarding shipping and seafarers. In this study, annual surveys from 1991 to 2023 (32 in total as there was no survey in 2020 due to COVID-19) were each interpolated onto a regular 10 × 10 m grid using a cubic triangulation method, which covers the inlet region with around 3 × 10^6 m^2. Beyond the surveyed inlet region, shoreface bathymetry was sourced from the most recent UKHO survey (which are undertaken far less frequently) and when possible, were supplemented with Lidar data (covering the inter- and supratidal zone) from the same or adjacent year. The seaward boundary of the ebb-tidal delta was identified by slope analysis, where the ebb-delta edge is defined by a steeper slope (associated with the sediment deposit) that meets a sharp change to the shallower slope of the upper shoreface (Fig. 1D). The up- and downdrift extent was determined where the temporal variation in the ebb-delta boundary reached a minimum, and the landward extent was defined by the fixed land configuration (Fig. 2). The channel thalweg was extracted as the divide between up- and downdrift units, which was extrapolated to the grid boundary on the basis of maximum slope (Burningham and French, 2006). The contours of 1.5, 0 and −1.5 m were extracted to show the positions of high, mean, and low tide levels.

In this research, the positive residual ('no-delta') approach (Stauble, 1998) was used for volumetric analysis (see Burningham and French (2006)). Volume changes were calculated only within the ebb-tidal delta boundary to exclude the changes in the wider shoreface. The delta extents differ year to year, as do the areas of the up- and downdrift constituent parts. Transition through the bypassing cycle is evaluated here based on the changing volumetric distribution within the inlet system, including consideration of the vertical framework, for which the ebb-tidal delta was sliced into 1.5 m interval layers that approximate to

Fig. 2. The bathymetries of the Deben inlet between 1991 and 2023. Ordnance Datum (OD) Newlyn was used as the vertical reference.

sub-tidal, low intertidal, high intertidal, and supra-tidal zones.

3.2. Wave and tidal condition analysis

Wave climate generated through the European Centre for Medium-Range Weather Forecasts (ECMWF) was used to capture changing wave conditions. ERA5 is the fifth generation ECMWF atmospheric reanalysis of the global climate from 1940 to the present, providing hourly estimates of oceanic climate variables at a 30 km spatial resolution that are interpolated to give data at a specific point chosen by users. Hourly wave data were used here covering the period from 1st April 1990 to 31st March 2023. Bathymetric surveys are generally undertaken in March/April, so a morphodynamic-year was established from 1st April in the previous year to 31st March in the year of the survey. Annual metrics representing the metocean climate thus used the same year. The wave variables extracted were H_s (Fig. 1B), T_p (Fig. 1C), and wave direction. Wave parameters were also divided into four-direction sectors, the northeast (NE: 0°-90°), southeast (SE: 90°-180°),

southwest (SW: 180°-270°) and northwest (NW: 270°-360°). In each morphodynamic-year, the direction frequency (Freq) and the mean, 75th and 95th percentile and maximum of H_s and T_p were calculated within these four-wave sectors. Timescales considered include the morphodynamic-year (Yr), half-year (summer (Sum): Apr-Sep, winter (Win): Oct-Mar) and three months (AMJ: 4–6, JAS: 7–9, OND: 10–12, JFM: 1–3). The North Atlantic Oscillation (NAO) index (sourced as a daily PCA-based index produced by NOAA Climate Prediction Center) was also used as an expression of the broader climate system, and calculated here as annual, summer, winter, and per three-month indices.

Hourly tide data over this time-scale is not available for the Deben, and those available for two neighbouring tidal gauges, Harwich (51.9480° N, 1.2921° E) and Lowestoft (54.4730° N, 1.7508° E), are not continuous over the full period. In January 2022, an autonomous pressure logger was installed at Bawdsey Quay at the mouth of the Deben estuary. Total pressure, recorded at 15 min intervals is compensated for atmospheric pressure using weather station records from Wattisham (20 km inland) and the residual pressure associated with the head of water is converted to water level relative to Ordnance Datum (OD) Newlyn. A modelled time series for Bawdsey Quay was generated by using the function fitting artificial neural networks (ANN) on the long-term (but intermittent) Harwich and Lowestoft records; the Root Mean Squared Error (RMSE) of the modelled time series is ±0.08 m, but the absolute error on annual mean, max, and the 75th and 95th percentile tidal level lies in the range 0.001–0.012 m. The function-fitting neural network belongs to the category of feedforward networks, specifically designed to model input-output relationships (Ahmad AL-Allaf, 2012). The 1991–2023 time series of tide levels used here are combined modelled and measurements, and refer to absolute water levels comprising both astronomical tides and meteorological surges. From these data, the mean, maximum, and 75th and 95th percentiles of tidal levels were computed. Furthermore, high-energy wave climates (frequency, 75th and 95th percentiles, and maximum of H_S) in the different direction sectors were analysed in the three-hour windows around high (HTide) and low (LTide) tide conditions.

3.3. Statistical analysis

Several statistical approaches were used here. The self-organizing map (SOM), a kind of artificial neural network method (Kohonen, 1982a, 1982b), was applied to wave climate variables (36 in total covering the frequency and annual mean, 75th, 95th percentiles and maximum of H_S and T_P in each of the NE, SE, SW and NW sectors) to examine the interannual shifts in NE-SW forcing. SOM has good performance in clustering, classification, and data mining (Kohonen, 2001). Typically in SOM, the network learns on its own to cluster data intelligently by spotting different patterns, rather than following preset solutions (Kalteh et al., 2008), and SOM's are widely used in the classification of climate patterns in order to explain climate variability (see for example Goharnejad et al. (2022), Izaguirre et al. (2012), Wolski et al. (2018)). Further explanation of the SOM approach for clustering is provided in Kohonen (2001) and Kalteh et al. (2008). In this paper, we used 4 neurons (2 × 2 topography) in the SOM to capture commonalities in annual wave climate over the 1991–2023 period.

A Pearson correlation was used to analyse the interactions between volume and change in the ebb-delta system, and metocean climate forcing. A total of 254 wave, tide, wave-tide interaction, and NAO parameters were correlated with 18 volumetric measures.

4. Results

4.1. Morphodynamic behaviour

The multi-annual bathymetries from 1991 to 2023 of the Deben inlet capture the latter stages of one bypassing cycle (which started in 1982, before annual hydrographic surveys began) and a complete cycle from 2003 to date (Fig. 2). Between 1991 and 1999, the updrift shoal extended southward, during which time the ebb jet deflected by about 50° clockwise. This led to erosion of the downdrift shoal and then margin as the ebb-channel route became increasingly extended. Notably, the ebb jet direction specifically shifted from southeast to south during the period 1995–1999 following a distinct growth in the updrift shoal. In 2000, the updrift shoal started to disintegrate, and over the following two years a new channel developed here whilst the existing ebb jet continued to bend toward the downdrift coast (rotating a further 50° clockwise) where it became increasingly narrow and shallow. The main ebb channel occupied a new position in 2003, breaching the pre-existing updrift shoal, thereby rotating back around 110°. The new bypassing cycle then started.

In the first two years of the new cycle, the ebb jet rotated in the updrift direction. The bed level change between 2003 and 2006 shows that the ebb channel deepened, and the updrift shoal narrowed and grew vertically. In 2006, a subtidal bar formed in the distal ebb jet area which made the ebb jet 'correct' its direction by shifting to the south of this bar. The resulting morphological state in 2006 is like 1991. Over the next 5 years, the updrift shoal grew southward and deflected the ebb jet to the south. Empirically, the cycle was in line to enter the unstable state where the updrift shoal fragments in advance of permanent breaching. In 2013, a small channel (known as locally as swatchways or fisherman's channels) developed across the north end of what had become a very robust updrift shoal. In the subsequent 5 years, a southeast-extending spit developed on the updrift side of this swatchway leading to a two-channel ebb-delta, whereby flow was still concentrated in the southern channel. The ebb-jet continued to rotate clockwise so that by 2021, the main ebb channel followed the main downdrift shoreline (as in the late-stage of the previous cycle).

Swatchways develop at various stages in the cycle and appear to be marginal flood channels (sensu lato Hayes, 1980) that form close to the Bawdsey foreland, as seen in 1991–92, 1995, 1999–2000 and 2013, but haven't previously persisted or developed into the new main tidal channel. The 2013 to 2019 period exhibited behaviour that was not evident in the previous cycle whereby the inlet comprised two distinct channels, and a divided updrift shoal. The north portion of this grew southward, but as the secondary channel persisted, the bank extended seaward, parallel with and then laterally overlapping the south updrift shoal. The secondary channel was finally compromised in 2019 when the extended north updrift bank pushed westward to weld with the south portion. This prompted another breach and a new channel forming across the north updrift shoal. Over the next two years, this new channel deepened, and the main tidal flow finally shifted to this channel in 2023.

4.2. Volumetric analysis

The volume and area changes in the ebb-tidal delta are compared in Fig. 3. The annual total volume and area of the ebb-tidal delta have generally increased over the last 33 years; this is largely due to growth in the updrift shoal which, by 2022, dominated the inlet region. The volume and area of the updrift shoal exhibit a stepwise growth which seem to be driven by large-scale sediment influx (lasting 1–3 years) occurring every 4–6 years. There were five (P1–5) significant sediment influx periods. During the P1 (1995–1996), a total of about 6.5×10^5 m^3 of sediment was added to the ebb tidal delta, and over 65 % of it was added in the updrift unit. In the next period P2 (2000–2003), about 3.9×10^5 m^3 sediment was deliver to the inlet, and in P3 (2005–2007) around 5.6×10^5 m^3 sediment was captured by the updrift shoal. A similar pattern continued in P4 (2010–2011) and P5 (2016–2018) when the downdrift shoal eroded whilst the updrift shoal volume increased by 5.1×10^5 m^3 and 4.3×10^5 m^3, respectively. The relative distributions in area and volume between the up- and downdrift shoals increases through the bypassing cycle as the channel progressively moves closer to the downdrift shoreline. Despite the ebb-delta being larger at the end of the more recent cycle, the relative distribution was less skewed at the point

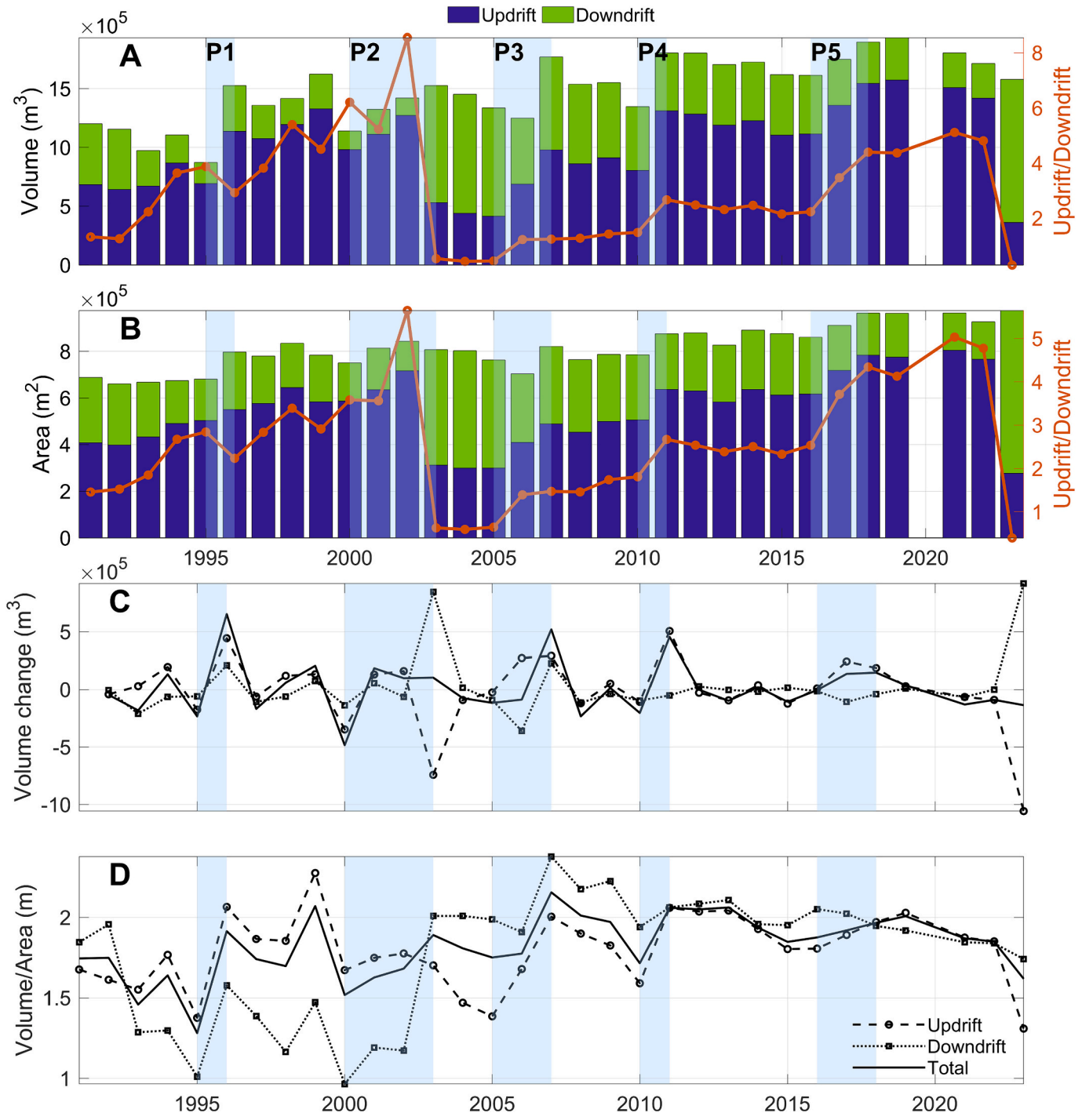

Fig. 3. Morphometric analysis of the Deben ebb-tidal delta, showing A) volume, B) area, C) volumetric change year to year, D) the ratio between volume and area of the total delta, up-, and downdrift shoals. In A) and B), the right y-axis represents the relative volume and area between up- and downdrift units. The shaded sections mark the periods of significant sediment influx (P1–5).

of bypassing in 2022/23 in comparison to 2002/03.

In intervening periods, the ebb-tidal delta exhibited an erosion state. From 1991 to 1995, the total sediment volume decreased around 3.3 × 10^5 m^3, due to the erosion of the 1993 downdrift shoal and then erosion of the 1995 updrift shoal. It is worth noting that the largest decrease (around 4.8 × 10^5 m^3) was observed in 2000, where 72 % was attributed to erosion of the updrift shoal. During the periods 2003–2005 and 2018–2023, although the whole delta experienced sediment loss, the magnitude of change was small. Over the period 2007–2010, around 4.2 × 10^5 m^3 of sediment was lost, mostly on the downdrift shoal; between 2011 and 2016, the erosion mainly occurred on the updrift shoal.

Overall, due to more sediment being imported than lost from the inlet, the ebb-tidal delta volume grew, and this is more pronounced on the updrift shoal. The ebb-delta volume in one year is strongly correlated (autocorrelation $R > 0.6$) with the volume of the previous or following year, but no other autocorrelation lags are evident. The rate of growth in the updrift shoals through the 2003–2023 cycle was 57.4 × 10^3 m^3/yr whilst the rate of loss in the downdrift shoals was 34.5 × 10^3 m^3/yr. The ebb-delta is holding on to more sediment than it is bypassing; this imbalance in the previous (1982–2003) cycle was around 8.5 × 10^3 m^3/

yr (Burningham and French, 2006) whilst in the recent cycle the net rate of ebb-delta growth was 23 × 10^3 m^3/yr. But the amount of sediment bypassed to the downdrift shoreline at the end of the cycle has remained comparable at 8.5 × 10^5 m^3 in 2003 and 9.2 × 10^5 m^3 in 2023.

The ratio between volume and area provides an expression of the average sediment distribution within the system, which again highlights episodes of sediment influx to the ebb-delta that are largely associated with the updrift shoal. The downdrift shoal behaved quite differently until 2011, and was notably lower than updrift, but the structure has since become more stable and consistent across the system. To explore these structural changes further, multi-layer volumes (Fig. 4) were calculated by slicing the depths from −3 m to 3 m with a 1.5 m interval, with a further two layers covering ≤−3 m and >3 m. Vertically, the subtidal zone (≤ −1.5 m) controls the volume changes. The stepwise growth is variable across the vertical structure and through time, but it plays a prominent role in the growth of the lower foreshore of the updrift shoal. Change in the downdrift shoal across any vertical layer is more progressive through time, aside from the breaching in 2003. As the ebb-channel divide between up- and downdrift moved, this was the primary driver of the simultaneous decrease and increase in up- and downdrift subtidal and lower foreshore volume, whilst any loss in the upper foreshore associated with the bypassing was balanced by a supply gain closer to updrift margin. The downdrift subtidal zone lost much of this additional volume within 5 years of the breach as the channel rapidly rotated from southeast back to south directed. This also aligned with the downdrift foreshore and supratidal increase in sediment volume over P3 as bypassed material was rapidly moved onshore and accumulated in elevated berms and ridges. In the subsequent years as the new bypassing cycle progressed, the updrift supratidal volume gradually increased whilst the downdrift supratidal gradually declined. The updrift upper foreshore exhibited a notably pulsed behaviour of short-term growth and decline in the years between breaching, especially the significant volume increase in the 2012–2014 period.

4.3. Wave climate analysis

Interannual wave climate was clustered into four groups (A, B, C and D) by the SOM method. Of the 36 annual wave statistics used in the SOM, significant differences (supported by $p < 0.01$ in the post-hoc Kruskal–Wallis test) were observed in 21 metrics across the four clusters (Fig. 5). The wave climate of cluster A is characterised by low frequency and low H_S and T_P of SW waves (Fig. 5c, g, k, n, q and u) and to a lesser extent energetic NE waves (Fig. 5a, e, i and s). Cluster B has significantly higher values in the NW waves (Fig. 5d, h, l, o and r), and to a lesser extent lower values in the SE wave variables (Fig. 5b, f, j, m, p and t). Cluster C is mostly characterised by larger easterly waves, and significantly those from the SE (Fig. 5f, j and p); cluster D represents the higher energy part of the southerly wave climates, and significantly those from the SW (Fig. 5c, k, n, q and u) but also captures the lowest energy in the NE wave climate (Fig. 5a, e, i and s). The distinct wave climates drawn out in the clustering provide evidence of interannual variability in wave forcing (Fig. 6); most prominent in this is the contrast

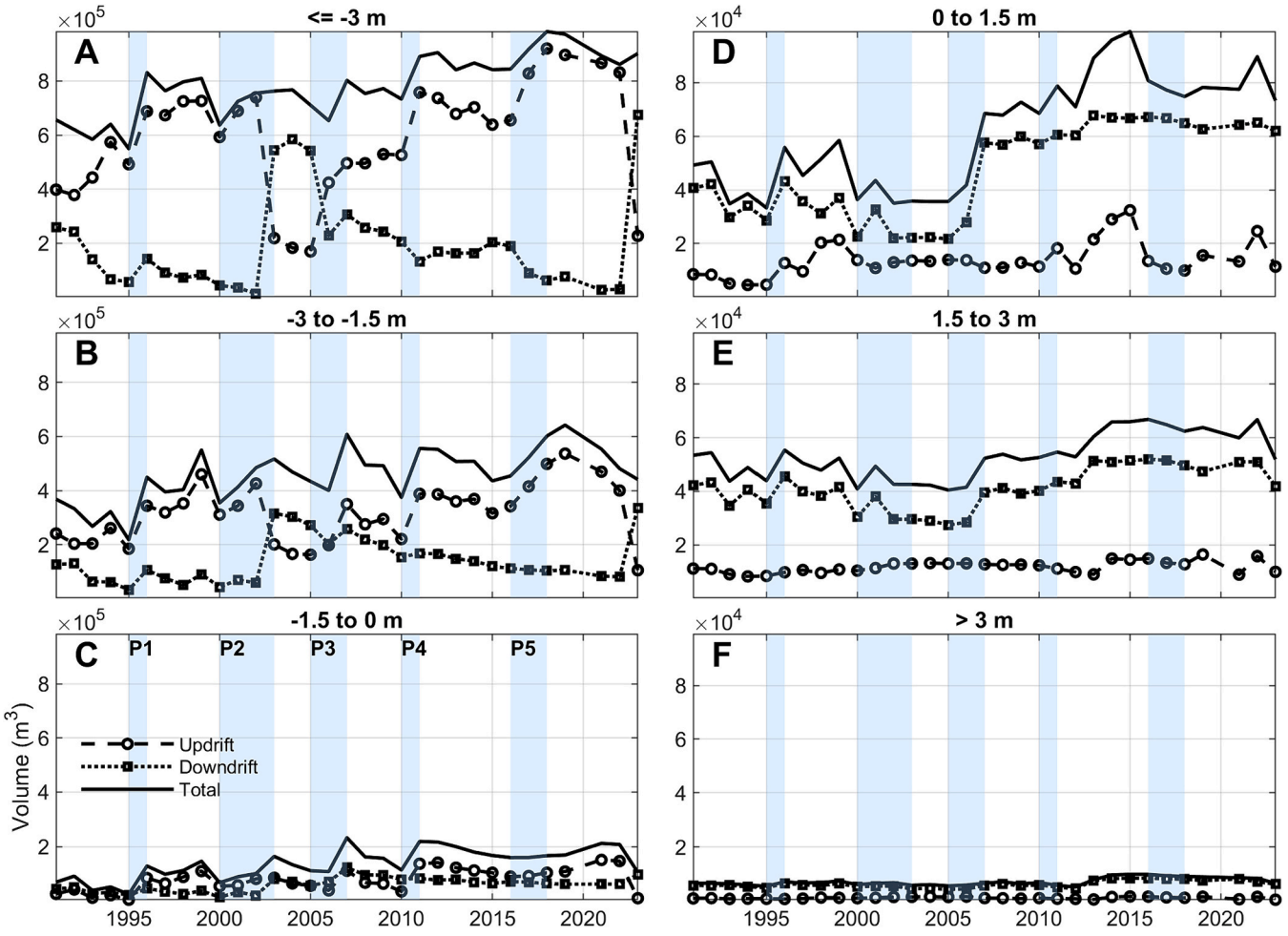

Fig. 4. Vertical structure of volumetric change in the ebb-tidal delta, A-F) showing each of the 1.5 m elevation intervals; left column is below mean sea level and right column is above mean sea level. The shaded sections mark the periods of significant sediment influx (P1–5). Note varying y-axis scales: A-C) are an order of magnitude greater than D-F).

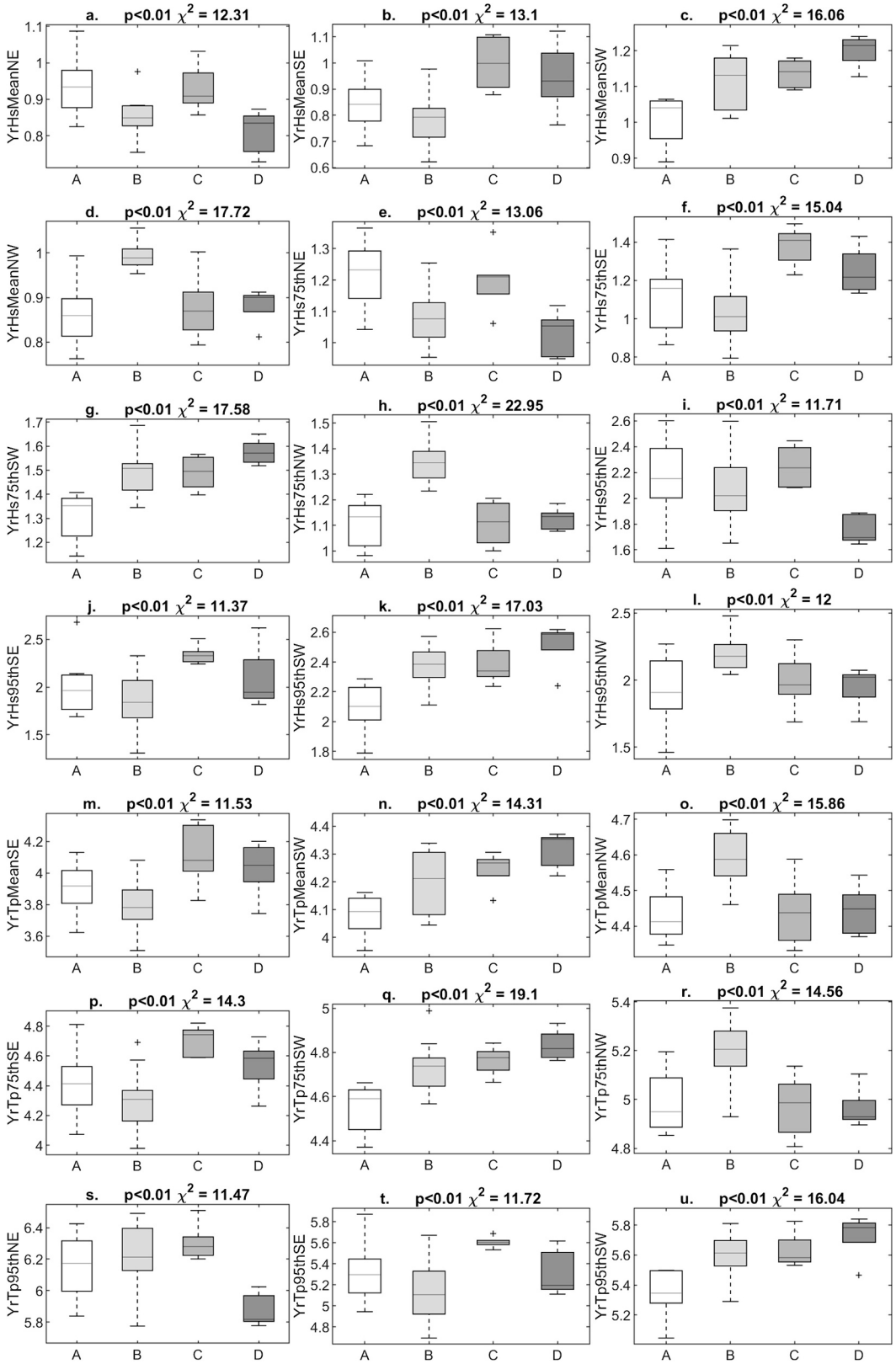

Fig. 5. Boxplots of the SOM clusters of annual wave climates. a-u) are a subset of the wave variables shown here with $p < 0.01$ in the post-hoc Kruskal–Wallis test.

between cluster A (low SW waves, higher average NE waves) and cluster D (low NE waves, high SW waves).

4.4. *Wave climate clusters vs volumetric analysis*

The timing of the wave climate clusters relative to change in ebb-tidal delta volume, reveals that most of the years previously defined as sediment influx periods are aligned with cluster A (Fig. 6). This is

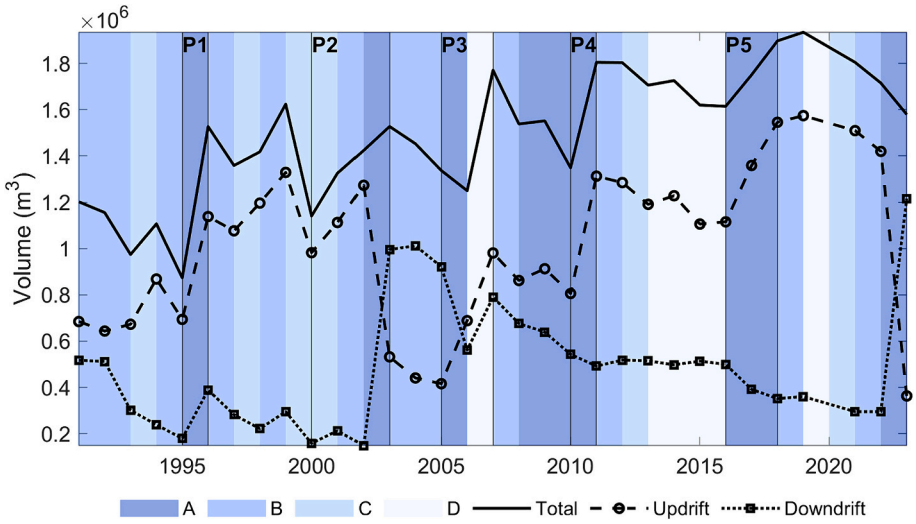

Fig. 6. Annual wave climate clusters (A relating to larger NE waves, B capturing larger NW waves, C from the SE, and D from the SW) vs ebb-tidal delta volumetric analysis. The boundaries of the significant sediment influx periods (P1–5) defined in the volumetric analysis were marked by the vertical lines.

especially the case for influx periods P1, P4 and P5, demonstrating that sediment influx has a close relationship with reduced SW and increased NE wave forcing (the key characteristics of cluster A). The cluster A wave climate is specifically associated with volumetric increase in the updrift component and the decline in the downdrift component (and this is especially evident in the most recent bypassing cycle). Volumetric changes that take place during the cluster D wave climate (capturing the larger southerly waves and smaller NE waves) show common behaviour between up- and down-drift volumes, whereas change during cluster B (larger westerly energy) and C (larger easterly energy) wave climates are

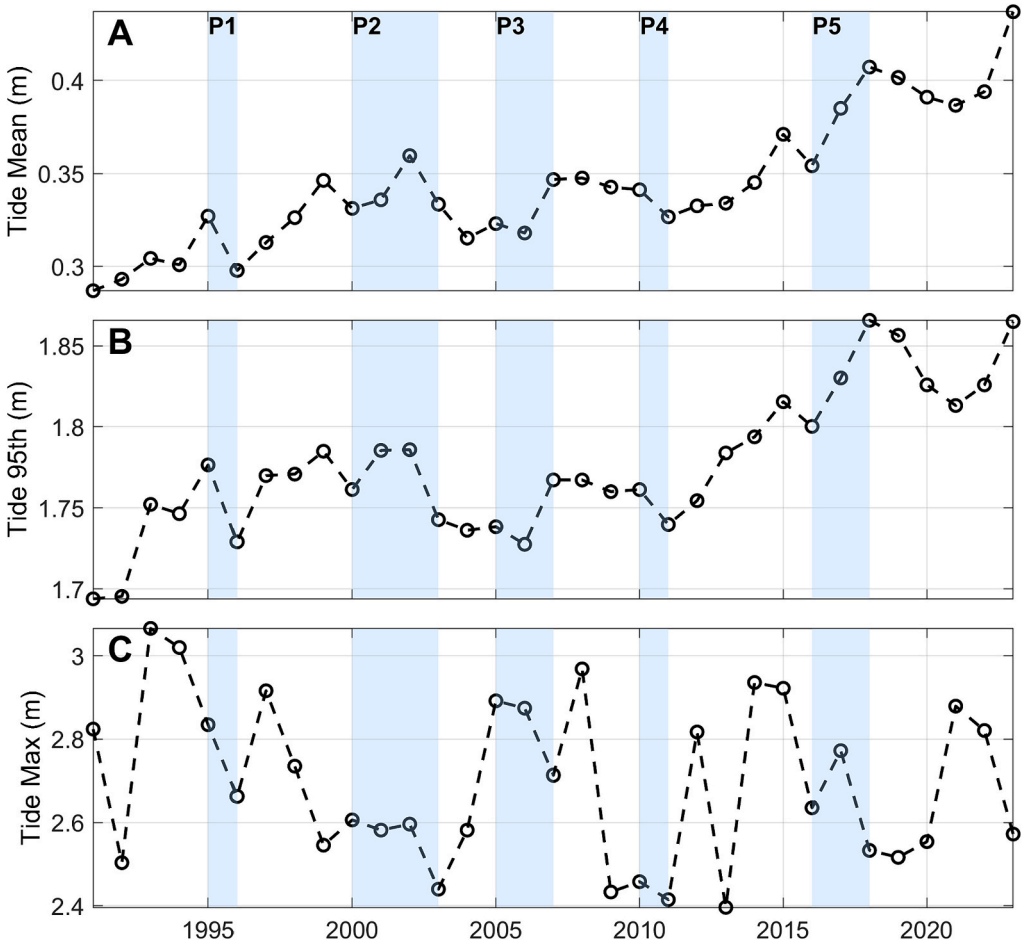

Fig. 7. The mean, 95th and max tide levels in the 1991–2023 period. The shaded sections mark the periods of significant sediment influx (P1–5). Ordnance Datum (OD) Newlyn was used as the vertical reference.

mixed. In fact, attributing volumetric behaviour to specific wave climates, beyond the link between sediment influx and increased NE wave energy, is complicated. Cluster B wave climate (greater westerly energy) is mostly linked to decreasing or stable volumes, whilst cluster C (larger easterly waves) is associated with increasing updrift volume in the former (until 2003) cycle but decreasing volume in the recent cycle (2003–2023). And the cluster D wave climate, although associated with increasing volume in the early stages of the recent cycle, has since been associated with periods of decreasing volume.

4.5. Tides

Annual tide level increased over the 1991–2023 period, evident in the mean and 95th percentile of the tide (Fig. 7). The mean tide level has increased 0.15 m, in the last 33 years, which equates to a mean water level rise of 4.5 mm/yr (1991 to present); the rate of sea-level rise at Lowestoft to the north is 2.69 ± 0.29 mm/yr over the period 1955–2022 (NOAA, 2022). Although there were no consistencies in the mean tide level within or between each influx period, the annual mean tide level increased significantly between 2011 and 2018, which aligns with the period when the ebb-tidal delta cycle stalled, and the inlet area became congested with multiple banks and channels. The maximum tide levels have fluctuated between 2.4 m and 3.1 m throughout these years, and there is limited specific association with influx periods which seem to align with the lower half of the range.

4.6. Climate-morphodynamic interactions

The interactions between sediment volume, and various statistical parameters of wave, tide, wave-tide conditions, and NAO indices were analysed by using a correlation matrix. The ebb-tidal delta volumes were split into up- and downdrift components, and into lower and upper layers of the sub-, inter-, and supratidal zones. A total of 254 metocean parameters (described in Section 3.2 and listed in Appendix A) were used in the correlation analysis with the 18 ebb-delta volume parameters. A correlation matrix subset is shown in Fig. 8, showing the 36 variables that exhibited a strong and significant correlation ($p \leq 0.05$ and $|R| \geq 0.4$).

Wave conditions correlate in part with the volume of the ebb-delta and its component parts, and these correlations are largely negative. Volumetric change in the updrift unit shows a negative correlation with frequency of summer (JAS) NE waves; the opposite association is seen in the downdrift unit which is positively correlated with the frequency of summer NE waves and negatively correlated with SW waves. Volume magnitude is also significantly correlated with the frequency of summer (SW) waves, positively in the updrift subtidal and downdrift intertidal and negatively in the downdrift subtidal. This contrast in direction of correlation between different vertical components captures the fact that the sub-, inter-, and supratidal parts of the system seem to respond in different ways to forcing.

The total ebb-tidal delta volume has moderate negative correlations with the summer (especially AMJ) NE extreme H_S. The updrift component is not significantly correlated with any wave measures, but downdrift is negatively correlated with the winter NE extreme (95th/max) wave H_S and T_P and summer (JAS) SE extreme H_S. Vertically, the updrift supratidal volumes are negatively correlated with easterly H_S metrics, and specifically those in the summer from the NE. The downdrift low inter- and subtidal layers have negative correlations with winter extreme NE wave H_S and T_P and summer (JAS) SE wave height.

The total and updrift ebb-tidal delta volumes are positively and strongly correlated to mean, 75th and 95th percentile tide levels. A clear separation in vertical response is also evident in both the up- and downdrift components whereby the lower updrift and the upper downdrift are positively correlated with tidal levels whilst the other units show no correlation.

Considering the interactions between wave and tide forcing, total

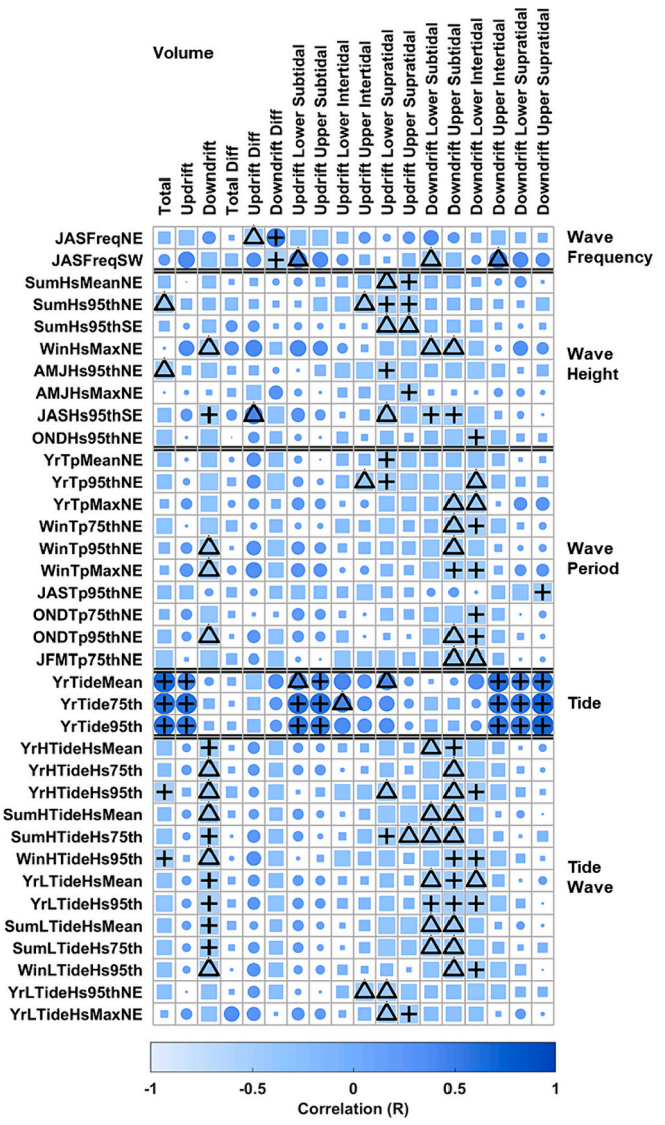

Fig. 8. Correlation matrix of ebb-tidal delta volume relative to metocean conditions. Although 254 metocean parameters were included in the correlation, just the subset (36 of the total) with strong ($|R| \geq 0.4$) and significant ($p \leq 0.05$) correlations are shown here. Filled circles represent $R > 0$, and filled squares represent $R < 0$; shape size represents $|R|$. This subset also was limited to only those variables that had >1 significant correlation at $p \leq 0.05$ (△) or at least 1 at $p \leq 0.01$ (+). The timescales include annual (Yr), summer (Sum: 4–9), winter (Win: 10–3) and three months (AMJ: 4–6, JAS: 7–9, OND: 10–12, JFM: 1–3). More details of parameters are provided in Appendix A.

delta volume is strongly and negatively correlated with high tide extreme H_S, especially in the winter. The updrift volume is not strongly correlated with any of the wave-tide interactions, but downdrift volume shows strong negative correlations with several wave-tide parameters, for various high and low tide, summer and winter extreme H_S. Within the vertical units, this wider range of negative correlations is evident across the lower part of the downdrift component, whilst the updrift supratidal shows some negative correlation with the size of larger waves at high tide. The only specific directions showing strong correlations, when combined with tide level, are extreme waves from the NE occurring at low tide, which are negatively correlated with the updrift upper delta. Despite tidal parameters exhibiting several strong positive correlations with ebb-delta volumes, the combined wave-tide interactions tend to be more closely linked to those associated with the wave climate.

In summary, larger (increased H_S and T_P) waves from the east (NE

and SE) tend to be associated with reduced ebb-tidal delta volume, particularly in the upper updrift and lower downdrift components; lower energy waves from NE/SE drive increased volume. The downdrift component of the ebb-delta is more responsive to changing wave conditions than the updrift which is more strongly correlated with tide level. The upper updrift is more responsive to the higher energy part of the summer NE wave climate (decrease in the larger summer NE waves is related to increased volume) whilst the lower downdrift is more directly linked to winter NE wave climate (reduction in larger winter NE waves is associated with increased volume). Elevated mean and high tide levels are associated with increased volume, especially in the lower updrift and upper downdrift components, and this is evidenced throughout the results as the ebb-tidal delta has grown in volume over the 33-year period and tide level has risen. The wave and tide conditions have discrete and independent effects on the ebb-tidal delta, whereas wave-tide interactions do not significantly change these underlying influences. The NAO indices show no correlation with ebb-delta morphodynamics.

5. Discussion

This work has quantified changes in the morphodynamics of a gravel-dominated ebb-tidal delta, based on multi-annual bathymetry, and annual metrics of wave and tidal forcing. Despite following a bypassing cycle (historically over a timescale of 10–30 years) that moves sediment from the up- to downdrift shoreline via shifting ebb delta shoals, change isn't always progressive. Morphological deviations in the cycle raise questions around what the primary drivers of inlet morphodynamics are, and what factors control cycle behaviour. The development and evolution of the swatchway from 2013 presented a sequence of morphological change that wasn't evident in the previous bypassing cycle. A double-channel system evolved, but a full breach completing the bypassing cycle did not materialise due to a) the growth of a spit updrift of this and b) limited south-southwest extension of the ebb-jet. Over the following 6 years, the spit fragmented and merged with the mid-shoal (still part of the updrift component), thereby achieving a partial bypass within the updrift region. The permanent breach and relocation of the main tidal flow to an up-drift course finally occurred in 2023, completing the cycle in 20 years. Whilst the result of the cycle is the same, and over a similar time scale, around half the cycle follows a different morphodynamic progression when comparing the 1990s and the 2010s.

Changes in the morphodynamic behaviour of an ebb-tidal delta cycle could be a common phenomenon that is simply undetected in more temporally limited datasets, particularly in larger or gravelly systems where bypassing cycles are in the order of decades in length. In the Ameland inlet within the barrier island chain of the Netherlands coast, Elias et al. (2019) found that a significant shift in sediment bypassing processes occurred in 1926. The large sandy ebb-tidal delta system, sustained by the large tidal backbarrier basin, experienced a shift from outer channel dynamics to main ebb-channel switching. This example shows that the predictability of cyclic behaviour is often limited, and subtle dynamics are difficult to capture in existing general empirical relationships and conceptual models (Elias et al., 2019).

Over the 30+ year period that we have sufficient bathymetric volumetric data, the ebb-delta has displayed a stepwise growth, and an associated large-scale sediment influx taking 1–3 years, every 4–6 years. A similar pulsed pattern of sediment influx was also found by Garel et al. (2019) in the mixed-energy and tide-dominated inlet of the Guadiana estuary that follows the Portugal - Spain border, flowing into the Gulf of Cadiz. They related the longshore sediment transport to the NAO and found that most of the largest transport rates (eastward at $>2 \times 10^5\ m^3/yr$) corresponded to strong negative phases of the winter NAO, which were associated with stormier wave conditions. O'Connor et al. (2011) analysed shoreline and ebb channel evolution at three embayed beaches in northwest Ireland between 1834 and 2008. They used the NAO index to represent the interannual variability in storminess and demonstrated that the fluctuations in average storminess may drive major changes in inlet configuration.

Storminess is widely considered a major factor in controlling the magnitude of longshore sediment transport, with the NAO evident as a strong indicator of winter wave energy; both are associated with shoreline sediment supply (Gulf of Cadiz, Spain; Plomaritis et al., 2015), nearshore bar and beach morphology (southwest England; Masselink et al., 2014), and spit progradation (southwest, France; Nahon et al., 2015). Although there is currently no evidence of a significant relationship between Deben inlet morphodynamics and the NAO, the broader association with metocean climate variability implies that longshore sediment supply and transport on varying time scales are linked to the NAO (Costas et al., 2016; Garel et al., 2019; Masselink et al., 2014; O'Connor et al., 2011; Poirier et al., 2017). The influence of the NAO and climate variability on the ebb-tidal delta cycles and bypassing processes is an intuitive assumption, but as demonstrated here, the link between climate and inlet morphodynamics is far more complicated than can be captured in the association with a single climate metric.

Segmentation of the annual wave climate into distinct climate clusters shows that, during sediment influx periods the frequency and size of SW waves is significantly suppressed relative to the other wave climate types, and the NE waves are larger (cluster A). The reduction in southerly wave forcing seems to permit greater efficiency in updrift ebb-delta growth, where sediment supplied by NE waves from the updrift shoreline contributes to volumetric and morphological change. As the ebb-delta sediment is coarse sand and gravel, this supply is primarily through the littoral zone, where this sediment resource in concentrated, but it is the subtidal zone that primarily benefits from the influx (Fig. 4). Although the low intertidal and subtidal zone of the neighbouring beaches is sand overlying a London Clay shore platform, the ebb-delta is gravel-dominated out to the extent of the deposit, at around 5 m below mean sea level, and sediment supply clearly contributes to gravel accumulation within this subtidal region of the ebb-delta.

The SW-dominated wave climate (cluster D) is only evident in the most recent cycle. There is no evidence to suggest that the SW waves are important for sediment delivery to the inlet, particularly given that the ebb-channel migration cycle describes a north-to-south bypassing process. But it is likely that SW waves inhibit or slow down the movement of sediment through the system. The most notable occurrence of the cluster D wave climate is during the mid 2010s, following a sustained cluster A climate and sediment influx period. The inlet morphodynamics embark on an unusual course resulting in the expansion of the updrift shoal, evolution of a second channel, and limited rotation of the main ebb channel that would permit the completion of a bypassing cycle. It's possible that southerly waves impeded movement in the ebb-jet region, forcing the ebb-delta to progress through a mini-bypassing cycle within the updrift shoal. This points to a varying role of the SW and NE wave climates within the bypassing cycle, which can trigger two different bypassing behaviours seen in the last two cycles (Fig. 9). Reduced SW wave forcing allows the updrift shoal to evolve rapidly, and as the ebb jet can shift southwesterly, the updrift shoal fragments before being finally breached. Greater SW forcing reduces the mobility of the ebb-jet region, and holds back a growing sediment resource updrift, allowing the development of a two-channel system.

The correlation analysis has shown that tide level has a significant positive correlation with size of the ebb-tidal delta, and in particular, its lower updrift and upper downdrift components. Although tidal currents are less associated with the transport of gravel in comparison to finer (sand/mud) sediments (Carter and Orford, 1993; Postma, 1990; Reading and Collinson, 1996), the low tide morphology of the Deben ebb-delta – which is dominated by low amplitude ebb-oriented gravel waves (Burningham and French, 2007) – is testament to the capacity of inlet tidal-currents to transport gravel. As such, it is no surprise that morphological changes in the Deben inlet are influenced by tides. According to morphodynamic modelling by Yin et al. (2019), utilizing the earlier cycle

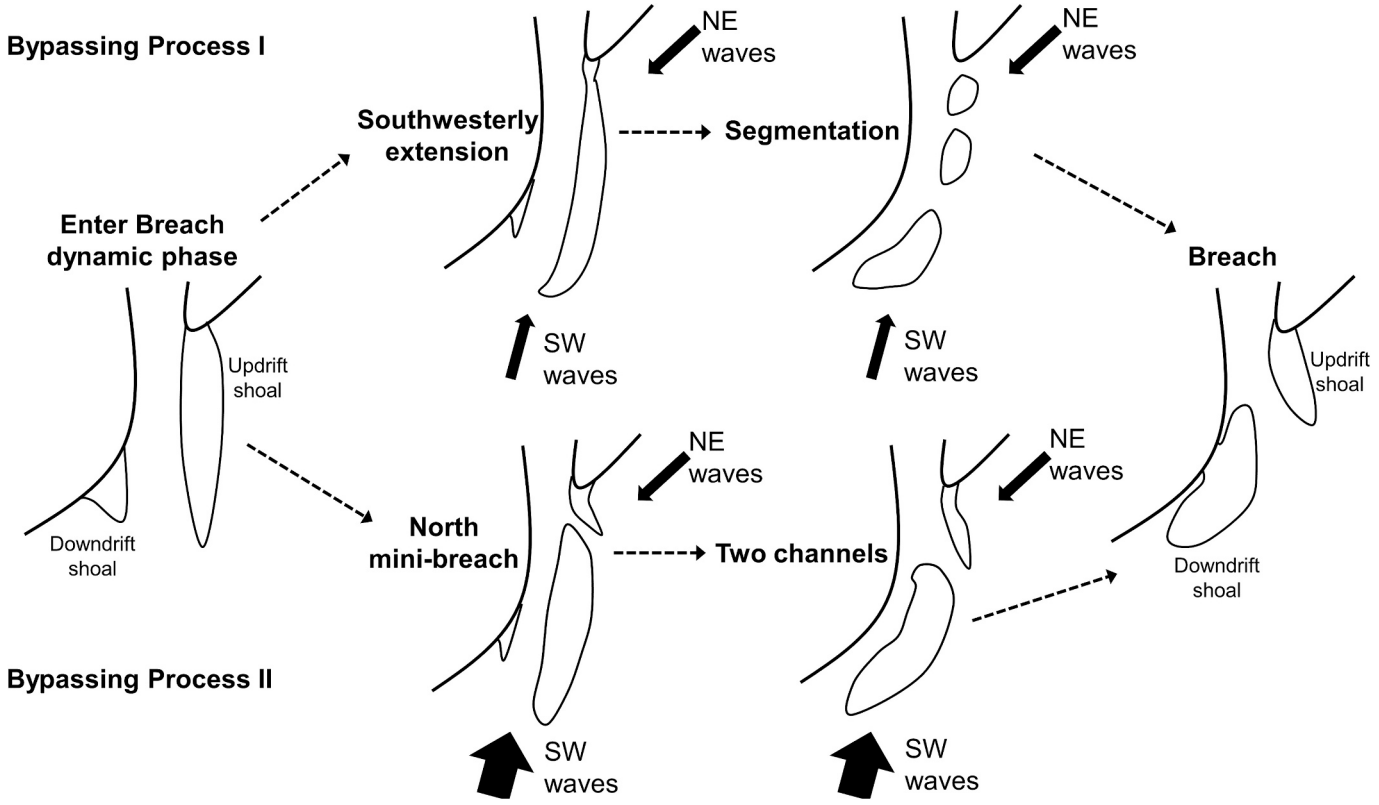

Fig. 9. Schematics of two different bypassing processes. NE waves drive sediment influx and the bypassing process. Bypassing Process I: lower SW waves; updrift shoal extend southwesterly; segmented; breach via fragment reorganization. Bypassing Process II: larger SW waves; ebb-jet movement limited; sediment accumulated in south updrift unit; mini-breach occurred in the updrift north end; developed two ebb channels; breach via channel switch.

(1991–2003) captured in the original bathymetric analysis (Burningham and French, 2006), the morphodynamic behaviour of Deben inlet is very sensitive to sea-level rise, which could change the cyclic pattern of bypassing. Lenstra and van der Vegt (2021) agreed that sea-level rise could impact the time scales of the cyclic behaviour of channel-shoal dynamics as the volume of ebb-tidal deltas is mostly directly attributed to tidal prism (Walton and Adams, 1976).

At the Deben, a rise of 10 cm in the tidal frame (on average between the two cycles) increases the tidal prism by 3.5 %; a 10 cm increase in the high tide level results in an increase of 8.8 % on the spring tidal prism. Most tidal prism – ebb delta volume models recognise that an increase in tidal prism and ebb-delta volume could extend the time scale of the bypassing cycle (Gaudiano and Kana, 2001; Lenstra et al., 2019). Whilst others have suggested that the morphodynamic cycle of the Deben ebb-delta is longer now than several decades ago (Simper, 1992: in Burningham and French, 2006), the two most recent cycles at the Deben were consistently in the region of 20 years (1982–2003 and 2003–2023). Despite interannual bathymetric detail from the last 33 years, we are still missing important pieces of information to determine whether cycle length is a changing variable and what this might be driven by, and this is where morphodynamic modelling might offer some insight.

In the Deben inlet, wave and tide forcing are more notable independent influences on ebb-tidal delta morphodynamics than in combination, and the specific aspects of wave climate that are important have varying impacts on the system. We see influx of sediment to the delta during years of suppressed SW and increased NE wave climate, but also that the updrift upper delta morphology is lowered by increased summer NE energy and downdrift lower delta morphology is lowered by increased winter NE wave energy. Despite weak correlations, there is a hint of positive association between NE wave energy and the updrift lower delta. This supports the result from the vertically sliced volume analysis that most of the sediment influx benefits the updrift subtidal, but also might reflect the fact that during stronger NE conditions, cross-shore processes move sediment from the upper delta to the lower delta.

Based on the modelling of sandy systems, Lenstra et al. (2019) proposed that waves drive shoal formation and channel deflection, and that subsequent shoal growth and delta breaching are attributed to the combined effect of waves and tides. They suggested that an optimum wave height exists for delta breaching in that larger waves are more likely to promote channel deflection rather than shoal breaching, which implies that large waves can operate as effective barriers to channel development across existing shoals. Burvingt et al. (2022) showed that asynchronicity in inlet sediment dynamics and wave forcing could be attributed to the geomorphological feedback on hydrodynamics, whereby the growth and migration of specific features can change the role and consequence of sediment-transporting wave-induced currents. Despite the considerable morphodynamic and climate forcing database developed for the Deben inlet, the ability to attribute key processes to specific morphological change at the multi-annual scale remains a challenge, possibly due to lag effects not only on specific processes, but also their interactions.

Karunarathna et al. (2016) applied the empirical orthogonal function model to the previous cycle and demonstrated that non-diffusive processes are important to the morphodynamic behaviour at the Deben inlet, based on the recognition of complex and uncorrelated trends in morphological change. They suggested this may be attributed to the combined effect of river inputs, tidal variation, wave climate changes and complex littoral processes but were unable to evidence this in the multiannual morphology and forcing parameters used, nor in the statistical modelling undertaken. In a wider study, Hicks and Hume (1996) investigated 17 sandy ebb-tidal deltas in New Zealand and found that these conformed to existing empirical models associating ebb-delta volume to tidal prism, the angle between the shoreline and ebb jet, and local wave climate and longshore sediment transport process. Whilst

the contemporary morphology of inlets and their ebb-deltas can be well explained within the context of the globally-derived empirical models and their envelopes of variability, these associations mask quite complex and geographically discrete morphodynamic responses that allude to the highly non-linear nature of sediment transport and meteorological forcing. There is an ongoing challenge to predict the evolution of ebb-tidal deltas (Lenstra et al., 2019; Zhu et al., 2019) that is highlighted well by the complicated relationships between morphodynamics and metocean climates demonstrated here for the Deben inlet. From this point of view, the physical processes involved in the morphological changes of Deben inlet, specifically in terms of interactions of waves from different directions with different ebb-delta configurations, requires further understanding and quantification.

6. Conclusion

Annual bathymetry, tides, and wave climate were investigated between 1991 and 2023 at the Deben inlet. Our results show that the ebb-tidal delta system can complete a bypassing cycle over a similar timescale, but via different progression of morphodynamics that reflect the varying wave, tide, and sediment supply processes. The multivariate multi-method approach followed here has established that inlet bypassing via the migration of ebb-tidal delta shoals and channels behave in different ways relative to the mutual interaction between forcing and morphology. On coastlines that exhibit strong bidirectionality in wave climate, there can be distinct interannual variability in wave forcing, but the influence that this has on ebb-delta morphodynamics can differ depending on stage in the bypassing cycle. Sediment influx to the system is associated with decreased SW and relative increase in NE wave forcing, and a gradual rise in the tidal frame is able to drive greater sediment transport within the system and thereby support a greater ebb-delta volume. Structurally, the upper and lower units of the up- and downdrift delta operate in opposing ways suggesting that cross-shore processes are active, with NE wave climate exerting a persistent but not necessarily coherent role on different parts of the system. The research demonstrates the challenges associated with seeking direct associations between morphological change and metocean forcing, but points to the need for more process-based studies, particularly in gravelly systems.

CRediT authorship contribution statement

Jie Gong: Writing – original draft, Visualization, Validation, Methodology, Formal analysis, Data curation, Conceptualization. **Helene Burningham:** Writing – review & editing, Supervision.

Declaration of competing interest

The authors declare that they have no known competing financial interests or personal relationships that could have appeared to influence the work reported in this paper.

Data availability

Data will be made available on request.

Acknowledgements

This research did not receive any specific grant from funding agencies in the public, commercial, or not-for-profit sectors. We thank John White (Deben Harbour Master) and Richard Tricker (Deben Marine Centre) for their assistance in installing the tide gauge, Trinity House for providing the sounding data, and the anonymous reviewers for their helpful comments.

Appendix A. Summary table of the metocean parameters were used in Fig. 8

Classes	Detail parameters	Count	Count (exclude NW cases)
Wave Frequency	(Yr + Sum + Win + AMJ + JAS + OND + JFM) × (NE + SE + SW + NW)	28	21
Wave Height	(Yr + Sum + Win + AMJ + JAS + OND + JFM) × (Mean + 75th + 95th + Max) × (NE + SE + SW + NW)	112	84
Wave Period	(Yr + Sum + Win + AMJ + JAS + OND + JFM) × (Mean + 75th + 95th + Max) × (NE + SE + SW + NW)	112	84
Tide	Yr × (Mean + 75th + 95th + Max)	4	4
Tide wave (without directions)	(Yr + Sum + Win) × (HT + LT) × (Mean + 75th + 95th + Max)	24	24
Tide wave (with directions)	Yr × (HT + LT) × (Freq + Mean + 75th + 95th + Max) × (NE + SE + SW + NW)	40	30
NAO	Yr + Sum + Win + AMJ + JAS + OND + JFM	7	7
In total		327	254

Appendix B. Supplementary data

Supplementary data to this article can be found online at https://doi.org/10.1016/j.geomorph.2024.109163.

References

Ahmad AL-Allaf, O.N., 2012. Cascade-forward vs. function fitting neural network for improving image quality and learning time in image compression system. In: Proceedings of the World Congress on Engineering 2012, WCE 2012, Vol II, 1172-1178. London, U.K.

Almar, R., Bergsma, E.W.J., Thoumyre, G., Baba, M.W., Cesbron, G., Daly, C., Garlan, T., Lifermann, A., 2021. Global satellite-based coastal bathymetry from waves. Remote Sens. (Basel) 13, 4628. https://doi.org/10.3390/rs13224628.

Balaga, A., 2006. Grain-size Trend Analysis of the Deben Estuary Inlet (MSc Freshwater and Coastal Science Thesis). UCL Department of Geography, London, U.K.

Beck, T.M., Wang, P., Li, H., Wu, W., 2020. Sediment bypassing pathways between tidal inlets and adjacent beaches. J. Coast. Res. 36, 897–914. https://doi.org/10.2112/JCOASTRES-D-19-00141.1.

Bertin, X., Fortunato, A., Oliveira, A., 2009. A modeling-based analysis of processes driving wave-dominated inlets. Cont. Shelf Res. 29, 819–834. https://doi.org/10.1016/j.csr.2008.12.019.

Bruun, P., Gerritsen, F., 1959. Natural bypassing of sand at coastal inlets. J. Waterw. Harb. Div. 85, 75–107. https://doi.org/10.1061/JWHEAU.0000152.

Burningham, H., French, J., 2006. Morphodynamic behaviour of a mixed sand-gravel ebb-tidal delta: Deben estuary, Suffolk, UK. Mar. Geol. 225, 23–44. https://doi.org/10.1016/j.margeo.2005.09.009.

Burningham, H., French, J., 2007. Morphodynamics and sedimentology of mixed-sediment inlets. J. Coast. Res. SI 50, 710–715 (Proceedings of the 9th International Coastal Symposium). Gold Coast, Australia. http://www.jstor.org/stable/26481678.

Burningham, H., French, J., 2017. Understanding coastal change using shoreline trend analysis supported by cluster-based segmentation. Geomorphology 282, 131–149. https://doi.org/10.1016/j.geomorph.2016.12.029.

Burvingt, O., Lerma, A.N., Lubac, B., Mallet, C., Senechal, N., 2022. Geomorphological control of sandy beaches by a mixed-energy tidal inlet. Mar. Geol. 450, 106863 https://doi.org/10.1016/j.margeo.2022.106863.

Carter, R.W.G., Orford, J.D., 1993. The morphodynamics of coarse clastic beaches and barriers: a short- and long-term perspective. J. Coast. Res. 15, 158–179. http://www.jstor.org/stable/25735728.

Costas, S., Naughton, F., Goble, R., Renssen, H., 2016. Windiness spells in SW Europe since the last glacial maximum. Earth Planet. Sci. Lett. 436, 82–92. https://doi.org/10.1016/j.epsl.2015.12.023.
De Swart, H.E., Zimmerman, J.T.F., 2009. Morphodynamics of tidal inlet systems. Annu. Rev. Fluid Mech. 41, 203–229. https://doi.org/10.1146/annurev.fluid.010908.165159.
Dodet, G., Bertin, X., Bruneau, N., Fortunato, A.B., Nahon, A., Roland, A., 2013. Wave-current interactions in a wave-dominated tidal inlet. J. Geophys. Res. Oceans 118, 1587–1605. https://doi.org/10.1002/jgrc.20146.
Elias, E.P.L., Hansen, J.E., 2013. Understanding processes controlling sediment transports at the mouth of a highly energetic inlet system (San Francisco Bay, CA). Mar. Geol. 345, 207–220. https://doi.org/10.1016/j.margeo.2012.07.003.
Elias, E.P.L., Cleveringa, J., Buijsman, M.C., Roelvink, J.A., Stive, M.J.F., 2006. Field and model data analysis of sand transport patterns in Texel Tidal inlet (the Netherlands). Coast. Eng. 53, 505–529. https://doi.org/10.1016/j.coastaleng.2005.11.006.
Elias, E.P.L., Van der Spek, A.J.F., Pearson, S.G., Cleveringa, J., 2019. Understanding sediment bypassing processes through analysis of high-frequency observations of Ameland Inlet, the Netherlands. Mar. Geol. 415, 105956 https://doi.org/10.1016/j.margeo.2019.06.001.
FitzGerald, D.M., 1982. Sediment bypassing at mixed energy tidal inlets. Coast. Eng. Proc. 18, 1094–1118. https://doi.org/10.9753/icce.v18.68.
FitzGerald, D.M., 1984. Interactions between the ebb-tidal delta and landward shoreline: price Inlet, South Carolina. J. Sediment. Petrol. 54, 1303–1318. https://doi.org/10.1306/212F85C6-2B24-11D7-8648000102C1865D.
FitzGerald, D.M., 1988. Shoreline erosional-depositional processes associated with tidal inlets. In: Aubrey, D.G., Weishar, L. (Eds.), Hydrodynamics and Sediment Dynamics of Tidal Inlets. Lecture Notes on Coastal and Estuarine Studies, 29. Springer, New York, NY, pp. 186–225. https://doi.org/10.1007/978-1-4757-4057-8_11.
FitzGerald, D.M., Buynevich, I.V., Davis, R.A., Fenster, M.S., 2002. New England tidal inlets with special reference to riverine-associated inlet systems. Geomorphology 48, 179–208. https://doi.org/10.1016/S0169-555X(02)00181-2.
Ford, M.R., Dickson, M.E., 2018. Detecting ebb-tidal delta migration using Landsat imagery. Mar. Geol. 405, 38–46. https://doi.org/10.1016/j.margeo.2018.08.002.
Garel, E., López-Ruiz, A., Ferreira, Ó., 2019. A method to estimate the longshore sediment transport at ebb-tidal deltas based on their volumetric growth: application to the Guadiana (Spain–Portugal border). Earth Surf. Process. Landf. 44, 2557–2569. https://doi.org/10.1002/esp.4679.
Gaudiano, D., Kana, T., 2001. Shoal bypassing in mixed energy inlets: Geomorphic variables and empirical predictions for nine South Carolina inlets. J. Coast. Res. 17, 280–291. http://www.jstor.org/stable/4300178.
Gaye, J., Walther, F., 1935. Die Wanderung der Sandriffe vor den ostfriesischen Inseln. Die Bautechnik 13, 555–567.
Geyman, E.C., Maloof, A.C., 2019. A simple method for extracting water depth from multispectral satellite imagery in regions of variable bottom type. Earth Space Sci. 6, 527–537. https://doi.org/10.1029/2018EA000539.
Goharnejad, H., Perrie, W., Toulany, B., Casey, M., Zhang, M., 2022. Clustering of climate change impacts on ocean waves in the Northwest Atlantic. J. Atmospheric Ocean. Technol. 39, 237–257. https://doi.org/10.1175/JTECH-D-21-0053.1.
Hayes, M.O., 1980. General morphology and sediment patterns in tidal inlets. Sediment. Geol. 26, 139–156. https://doi.org/10.1016/0037-0738(80)90009-3.
Hayes, M.O., FitzGerald, D.M., 2013. Origin, evolution, and classification of tidal inlets. J. Coast. Res. 69, 14–33. https://doi.org/10.2112/SI_69_3.
He, Y., Liu, X., Duan, Z., Liu, C., Hou, P., Lu, C., Wu, Y., 2022. Long-term morphodynamic evolution in the Modaomen Estuary of the Pearl River Delta, South China. Geomorphology 398, 108057. https://doi.org/10.1016/j.geomorph.2021.108057.
Hench, J.L., Luettich Jr., R.A., 2003. Transient tidal circulation and momentum balances at a shallow inlet. J. Phys. Oceanogr. 33, 913–932. https://doi.org/10.1175/1520-0485(2003)33<913:TTCAMB>2.0.CO;2.
Herrling, G., Winter, C., 2014. Morphological and sedimentological response of a mixed-energy barrier island tidal inlet to storm and fair-weather conditions. Earth Surf. Dyn. 2, 363–382. https://doi.org/10.5194/esurf-2-363-2014.
Herrling, G., Winter, C., 2018. Tidal inlet sediment bypassing at mixed-energy barrier islands. Coast. Eng. 140, 342–354. https://doi.org/10.1016/j.coastaleng.2018.08.008.
Hicks, D.M., Hume, T.M., 1996. Morphology and size of ebb tidal deltas at natural inlets on open-sea and Pocket-bay Coasts, North Island, New Zealand. J. Coast. Res. 12, 47–63. http://www.jstor.org/stable/4298459.
Hydrographic Office, 2000. Admiralty Tide Tables: United Kingdom and Ireland (Including European Channel Ports). Hydrographer of the Navy. Admir. Tide Tables U. K. Irel. Eur, Channel Ports.
Izaguirre, C., Menéndez, M., Camus, P., Méndez, F.J., Mínguez, R., Losada, I.J., 2012. Exploring the interannual variability of extreme wave climate in the Northeast Atlantic Ocean. Ocean Model. 59–60, 31–40. https://doi.org/10.1016/j.ocemod.2012.09.007.
Kalteh, A.M., Hjorth, P., Berndtsson, R., 2008. Review of the self-organizing map (SOM) approach in water resources: analysis, modelling and application. Environ. Model. Software 23, 835–845. https://doi.org/10.1016/j.envsoft.2007.10.001.
Karunarathna, H., Horrillo-Caraballo, J., Burningham, H., Pan, S., Reeve, D.E., 2016. Two-dimensional reduced-physics model to describe historic morphodynamic behaviour of an estuary inlet. Mar. Geol. 382, 200–209. https://doi.org/10.1016/j.margeo.2016.10.014.
Kohonen, T., 1982a. Analysis of a simple self-organizing process. Biol. Cybern. 44, 135–140. https://doi.org/10.1007/BF00317973.
Kohonen, T., 1982b. Self-organized formation of topologically correct feature maps. Biol. Cybern. 43, 59–69. https://doi.org/10.1007/BF00337288.
Kohonen, T., 2001. Self-organizing Maps. Springer-Verlag, Berlin. https://doi.org/10.1007/978-3-642-56927-2.
Lenstra, K.J.H., van der Vegt, M., 2021. The impact of sea-level rise and basin area reduction on the cyclic behaviour of tidal inlet systems. Cont. Shelf Res. 214, 104323 https://doi.org/10.1016/j.csr.2020.104323.
Lenstra, K.J.H., Ridderinkhof, W., Vegt, M., 2019. Unraveling the mechanisms that cause cyclic channel-shoal dynamics of Ebb-Tidal Deltas: a numerical modeling study. Case Rep. Med. 124, 2778–2797. https://doi.org/10.1029/2019JF005090.
Leonardi, N., Plater, A.J., 2017. Residual flow patterns and morphological changes along a macro- and meso-tidal coastline. Adv. Water Resour. 109, 290–301. https://doi.org/10.1016/j.advwatres.2017.09.013.
Luck, G., Witte, H.H., 1974. Erfassung morphologischer Vorgange der ostfriesischen Riffbogen in Luftbildern. Jber Forschungstelle Nord 25, 33–54.
Masselink, G., Austin, M., Scott, T., Poate, T., Russell, P., 2014. Role of wave forcing, storms and NAO in outer bar dynamics on a high-energy, macro-tidal beach. Geomorphology 226, 76–93. https://doi.org/10.1016/j.geomorph.2014.07.025.
McBride, R.A., Anderson, J.B., Buynevich, I.V., Byrnes, M.R., Cleary, W.L., Fenster, M.S., FitzGerald, D.M., Hapke, C.J., Harris, M.S., Hein, C.J., Johnson, C., Klein, A.H. da F., Liu, B., Menezes, J.T. de, Mulhern, J.S., Oliver, T.S.N., Pejrup, M., Riggs, S.R., Roberts, H.H., Rodríguez, A.B., Seminack, C.T., Short, A.D., Stone, G.W., Tamura, T., Wallace, D.J., Wang, P., 2022. Morphodynamics of modern and ancient barrier systems: an updated and expanded synthesis. In: Treatise on Geomorphology (second edition), 8. Elsevier, pp. 289–417. https://doi.org/10.1016/B978-0-12-374739-6.00279-7.
Nahon, A., Idier, D., Fenies, H., Mugica, J., Senechal, N., Mallet, C., 2015. Role of North Atlantic climate variability on barrier-spit oscillations: the cap ferret. In: The Proceedings of the Coastal Sediments 2015. Presented at the Coastal Sediments 2015, World Scientific, San Diego, USA. https://doi.org/10.1142/9789814689977_0240.
NOAA, 2022. Relative sea level trend 170-068 Lowestoft, UK. Available at: https://tidesandcurrents.noaa.gov/sltrends/sltrends_station.shtml?id=170-068. (Accessed 6 December 2023).
NRFA, 2024. National river flow archive: 53002 – Deben at Naunton Hall. https://nrfa.ceh.ac.uk/data/station/meanflow/35002.
O'Connor, M., Cooper, J., Jackson, D., 2011. Decadal behaviour of tidal inlet-associated beach systems, northwest Ireland, in relation to climate forcing. J. Sediment. Res. 81, 38–51. https://doi.org/10.2110/jsr.2011.3.
Oertel, G.F., 1988. Processes of sediment exchange between tidal inlets, ebb deltas and barrier islands. Hydrodyn. Sediment Dyn. Tidal Inlets 29, 297–318. https://doi.org/10.1007/978-1-4757-4057-8_17.
Plomaritis, T.A., Benavente, J., Laiz, I., Del Río, L., 2015. Variability in storm climate along the Gulf of Cadiz: the role of large scale atmospheric forcing and implications to coastal hazards. Climate Dynam. 45, 2499–2514. https://doi.org/10.1007/s00382-015-2486-4.
Poirier, C., Tessier, B., Chaumillon, E., 2017. Climate control on late Holocene high-energy sedimentation along coasts of the northeastern Atlantic Ocean. Palaeogeogr. Palaeoclimatol. Palaeoecol. 485, 784–797. https://doi.org/10.1016/j.palaeo.2017.07.037.
Posford Duvivier, 1999. Suffolk estuarine strategies: Deben Estuary. In: Strategy Report: Phase 2 Volume 1 Main Report, 5–20. Peterborough, UK, Environment Agency.
Postma, G., 1990. Depositional architecture and facies of river and fan deltas: a synthesis. In: Coarse-Grained Deltas, pp. 13–27. https://doi.org/10.1002/9781444303858.ch2.
Reading, H.G., Collinson, J.D., 1996. Clastic coasts. In: Sedimentary Environments: Processes, Facies and Stratigraphy. Blackwells, Cornwall, pp. 154–231.
Ridderinkhof, W., de Swart, H., van der Vegt, M., Hoekstra, P., 2016a. Modeling the growth and migration of sandy shoals on ebb-tidal deltas. Case Rep. Med. 121, 1351–1372. https://doi.org/10.1002/2016JF003823.
Ridderinkhof, W., Hoekstra, P., van der Vegt, M., de Swart, H., 2016b. Cyclic behavior of sandy shoals on the ebb-tidal deltas of the Wadden Sea. Cont. Shelf Res. 115, 14–26. https://doi.org/10.1016/j.csr.2015.12.014.
Simper, R., 1992. The Deben River: An Enchanted Waterway (English Estuaries). Creekside Publishing, ISBN 9780951992708.
Smith, J.B., FitzGerald, D.M., 1994. Sediment transport patterns at the Essex River Inlet ebb-tidal delta, Massachusetts, USA. J. Coast. Res. 10, 752–774. http://www.jstor.org/stable/4298268.
Son, C.S., Flemming, B.W., Bartholomä, A., 2011. Evidence for sediment recirculation on an ebb-tidal delta of the East Frisian barrier-island system, southern North Sea. Geo-Mar. Lett. 31, 87–100. https://doi.org/10.1007/s00367-010-0217-8.
Stauble, D., 1998. Techniques for measuring and analysing inlet ebb shoal evolution. Coast. Eng. Tech. Note 13.
Wallingford, H.R., 2002. Southern North Sea sediment transport study. Phase 2.
Walton, T.L., Adams, W.D., 1976. Capacity of inlet outer bars to store sand. Coast. Eng. 1919–1937 https://doi.org/10.1061/9780872620834.112.
Wolski, P., Jack, C., Tadross, M., van Aardenne, L., Lennard, C., 2018. Interannual rainfall variability and SOM-based circulation classification. Climate Dynam. 50, 479–492. https://doi.org/10.1007/s00382-017-3621-1.
Yin, Y., Karunarathna, H., Reeve, D.E., 2019. Numerical modelling of hydrodynamic and morphodynamic response of a meso-tidal estuary inlet to the impacts of global climate variabilities. Mar. Geol. 407, 229–247. https://doi.org/10.1016/j.margeo.2018.11.005.
Zhu, C., Guo, L., Maren, D. s, Tian, B., Wang, X., He, Q., Wang, Z.B., 2019. Decadal morphological evolution of the mouth zone of the Yangtze Estuary in response to human interventions. Earth Surf. Process. Landf. 44, 2319–2332. https://doi.org/10.1002/esp.4647.